Optimal tunneling enhances the quantum photovoltaic effect in double quantum dots

2014 New J. Phys. 16 045019

(http://iopscience.iop.org/1367-2630/16/4/045019)

New Journal of Physics
The open access journal at the forefront of physics
Deutsche Physikalische Gesellschaft DPG | IOP Institute of Physics

Optimal tunneling enhances the quantum photovoltaic effect in double quantum dots

Chen Wang[1,3], **Jie Ren**[2] **and Jianshu Cao**[1,3]

[1] Singapore-MIT Alliance for Research and Technology, 1 CREATE Way, Singapore 138602, Singapore
[2] Theoretical Division, Los Alamos National Laboratory, Los Alamos, New Mexico 87545, USA
[3] Department of Chemistry, Massachusetts Institute of Technology, 77 Massachusetts Avenue, Cambridge, MA 02139, USA
E-mail: wangchen@smart.mit.edu, renjie@lanl.gov and jianshu@mit.edu

Received 14 November 2013, revised 10 February 2014
Accepted for publication 21 February 2014
Published 25 April 2014

New Journal of Physics **16** (2014) 045019
doi:10.1088/1367-2630/16/4/045019

Abstract

We investigate the quantum photovoltaic effect in double quantum dots by applying the nonequilibrium quantum master equation. A drastic suppression of the photovoltaic current is observed near the open circuit voltage, which leads to a large filling factor. We find that there always exists an optimal inter-dot tunneling that significantly enhances the photovoltaic current. Maximal output power will also be obtained around the optimal inter-dot tunneling. Moreover, the open circuit voltage behaves approximately as the product of the eigen-level gap and the Carnot efficiency. These results suggest a great potential for double quantum dots as efficient photovoltaic devices.

Keywords: electronic transport in mesoscopic systems, photoconduction and photovoltaic effect, quantum dots, quantum description of interaction of light and matter

1. Introduction

As fossil-fuels, currently the main energy suppliers in our modern society, get scarcer and more expensive, renewable energies are becoming increasingly important and desirable. To meet this

demand, solar energy, a significant green energy source, attracts a broad spectrum of attention both from industrial applications and fundamental research [1]. In particular, the photovoltaic effect, first discovered by E Becquerel in 1839, is a potentially promising technology for light harvesting that converts our inexhaustible supply of sunlight to electricity for performing useful work.

Great efforts have been made to design efficient semiconductor-based solar cells [2]. However, the energy efficiency obtained is still too low to meet daily human needs. The main reason for this is that the excess excitation energy of the electron-hole pair above the energy gap is wasted through thermal phonon emission. By adding multiple impurity levels, M Wolf expected photovoltaic enhancement for the low energy spectrum collection [3]. Meanwhile, Shockley and Queisser suggested that the included impurity would also have a corresponding strengthening effect on the recombination process [4], resulting in no improvement of the photovoltaic current. Moreover, there have been various other proposals to enhance solar conversion efficiency [5–9]. Recently, quantum dots (QDs) have emerged as alternative candidates to fabricate solar cells, due to their ability to enhance photon harvesting via a multi-level structure [10, 11]. The novel feature of QD is that by adjusting the dot size, the energy scale of the excitation gap can be tuned across a wide regime, which extends the absorption spectrum down to the infrared range [12] and makes QD competitive in designing multi-junction solar cells.

In particular, the influence of quantum coherence in improving photovoltaic efficiency has been addressed by M O Scully *et al* [13, 14]. They studied photovoltaic cells as quantum heat engines modeled by electronic level systems resonantly coupled to multi-reservoirs with biased temperatures, which convert incoherent photons to electricity. Based on the full quantum master equation, which includes quantum coherence represented as off-diagonal density matrix elements, the photovoltaic current shows astonishing enhancement compared to its counterpart from population dynamics in the classical limit. This concept has also been extended to photosynthetic heat engines, which convert solar energy into chemical energy [15–20]. From a theoretical point of view, these generalized engines share the same underlying mechanism.

Considering the importance of quantum coherence in energy conversion for quantum photovoltaic systems, we apply the quantum master equation to study the quantum photovoltaic effect in a double quantum dot (DQD) system, which can also be regarded as a donor-acceptor system. In particular, the parallel sandwiching of many DQDs between electronic leads may have benefits such as flexible scalability and tunability for this kind of nanoscale photovoltaic device. We pay special attention to the three crucial ingredients of photovoltaic applications: short circuit current, open circuit voltage and extractable output power, and analyze the ability of the dots to convert photons into electricity. Our results show that there exists an optimal inter-dot tunneling that significantly enhances the quantum photovoltaic current and output power. Moreover, the open circuit voltage behaves approximately as the product of the eigen-level gap and the Carnot efficiency. As a result, maximal output power will be obtained around the optimal inter-dot tunneling. The work is organized as follows: in section 2, we describe the model of DQDs and obtain the solution of the quantum master equation. In section 3, we present results and corresponding discussions regarding the quantum photovoltaic effect and current enhancement at optimal tunneling. A concise summary is given in the final section.

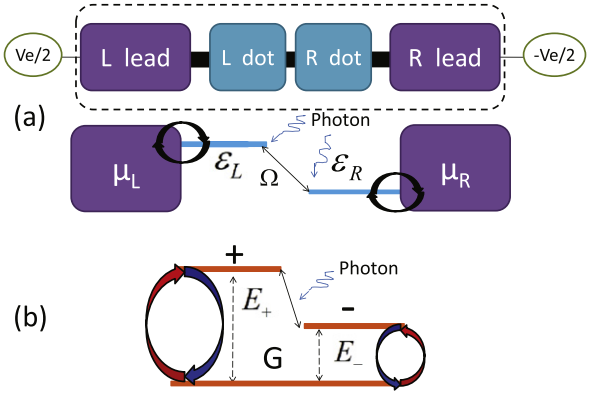

Figure 1. (a) Schematic illustration of the DQD device and its photovoltaic dynamics in real space: the electron hops between the left (right) dot and the left (right) lead, and between the left and right dots; the photon field interacts with the electron population difference of two dots. (b) Scheme of the DQD dynamics in eigen-space: the photon absorption (emission) assists the excitation (relaxation) between the eigen-state $|-\rangle$ and $|+\rangle$; the excitation (relaxation) between the ground state $|G\rangle$ and the superposition state $|+\rangle$ or $|-\rangle$ are accompanied by the electron hopping from (to) two electronic leads to (from) the DQD.

2. Model and method

In this section, the model of DQD coupled both to electron reservoirs and solar environment is first introduced in part 2.1. Then the quantum master equation is derived in part 2.2 by assuming that the system-reservoir couplings are much weaker than the energy gap of DQD. Finally, in part 2.3 the analytical expressions of steady state electron and photon currents are exhibited.

2.1. Hamiltonian

The photovoltaic system is described by a DQD coupled to two separate electronic reservoirs (see figure 1(a)), with the total Hamiltonian: $\hat{H} = \hat{H}_D + \sum_{v=L,R}\left(\hat{V}_v + \hat{H}_v\right) + \hat{V}_{D-ph} + \hat{H}_{ph}$. $\hat{H}_D$ denotes the central DQD by

$$\hat{H}_D = \epsilon_L \hat{d}_L^\dagger \hat{d}_L + \epsilon_R \hat{d}_R^\dagger \hat{d}_R + \Omega\left(\hat{d}_L^\dagger \hat{d}_R + \hat{d}_R^\dagger \hat{d}_L\right), \tag{1}$$

where $\hat{d}_{L(R)}^\dagger$ creates one electron on the $L(R)$ QD with energy $\epsilon_{L(R)}$, and Ω denotes the inter-dot tunneling between L and R, which both can be flexibly tuned via gate voltages applied on the dots [21]. Without loss of generality, we consider the strong Coulomb repulsion limit so that the system has three states: the left dot occupied state $|L\rangle$, the corresponding right one $|R\rangle$, and the ground state $|G\rangle$ with both dots empty. $\hat{H}_{L(R)}$ depicts the $L(R)$ electronic lead through $\hat{H}_v = \sum_k \epsilon_{k,v} \hat{c}_{k,v}^\dagger \hat{c}_{k,v}$, with $\hat{c}_{k,v}^\dagger$ creating one electron with energy $\epsilon_{k,v}$ and momentum k in the lead v.

$$\hat{V}_v = \sum_k t_{k,v} \hat{d}_v^\dagger \hat{c}_{k,v} + \text{H.c.} \tag{2}$$

gives the coupling between the dot v and the lead v, which conserves the total electron number, and t_{kv} is the system-lead tunneling strength. When the sun sheds light on the system, the DQD interacts with the photons in diagonal coupling form, described by

$$\hat{V}_{D-ph} = \sum_q g_q \left(\hat{a}_q + \hat{a}_q^\dagger\right)\left(\hat{d}_L^\dagger \hat{d}_L - \hat{d}_R^\dagger \hat{d}_R\right), \tag{3}$$

where $\hat{a}_q^\dagger$ generates one photon with frequency ω_q in the solar environment, modeled as $\hat{H}_{ph} = \sum_q \omega_q \hat{a}_q^\dagger \hat{a}_q$, and g_q is the coupling strength.

Here, we consider that the coupling between the photon environment and the polarization of electron populations on the DQD (instead of the off-diagonal interaction between dots) is the dominant mechanism. This type of electronelectron–photonphoton coupling has been found in DQDs [22, 23], and has already been extensively studied for similar electron-phonon coupling in such systems [24–28]. Distinct from the off-diagonal electronelectron–photonphoton coupling $\sum_q g_q \left(\hat{a}_q + \hat{a}_q^\dagger\right)\left(\hat{d}_L^\dagger \hat{d}_R + \hat{d}_R^\dagger \hat{d}_L\right)$, it does not seem obvious that equation (3) is able to produce the photovoltaic effect in the local basis. However, as we will show soon, by transforming the system into eigen-space (see also figure 1(b)), it is clear that the photon-assisted tunneling emerges with the help of inter-dot tunneling Ω in equation (1). This inter-dot tunneling, on the one hand assists the photovoltaic current, and on the other hand diminishes the photovoltaic current. Thus, an optimal inter-dot tunneling will be obtained to enhance the photovoltaic effect.

Such an optimal-tunneling-enhanced photovoltaic effect will not occur in the off-diagonal type of electron–photon interaction case $\sum_q g_q \left(\hat{a}_q + \hat{a}_q^\dagger\right)\left(\hat{d}_L^\dagger \hat{d}_R + \hat{d}_R^\dagger \hat{d}_L\right)$, which actually has a different physical behavior from the diagonal form at equation (3). The reason is that in the absence of inter-dot electron tunneling, there is no additional current leakage between two dots so that each electron hopping is fully accompanied by single photon emission or absorption. Therefore, the performance of the thermodynamic efficiency and the flux is high, as similarly described in the maser model [13]. While it is under finite and strong inter-dot electron tunneling, the electron transport is mainly controlled by downstream inter-dot tunneling, which severely offsets the photon-assisted photovoltaic current. Consequently, increasing the inter-dot electron tunneling will monotonically suppress the photovoltaic current and photon flux, and we do not have the same optimal performance as that which will be uncovered in the following.

To investigate the quantum evolution of the system density matrix, it is more convenient to work in the eigen-space of the DQD by diagonalizing equation (1):

$$\begin{aligned} |+\rangle &= \cos\frac{\theta}{2}|L\rangle + \sin\frac{\theta}{2}|R\rangle, \\ |-\rangle &= -\sin\frac{\theta}{2}|L\rangle + \cos\frac{\theta}{2}|R\rangle, \end{aligned} \tag{4}$$

are superpositions of the left and right occupied states, with $\tan\theta = 2\Omega/\Delta$ and $\Delta = \epsilon_L - \epsilon_R$ the inter-dot energy gap. The corresponding eigen-levels are

$$E_{\pm} = \frac{\epsilon_L + \epsilon_R}{2} \pm \frac{\sqrt{\Delta^2 + 4\Omega^2}}{2}. \tag{5}$$

The ground state $|G\rangle$ remains intact. This pre-diagonalization before applying the quantum master equation is important to make the treatment consistent with the second law of thermodynamics [29].

2.2. Quantum master equation

When the interactions of the DQD with the leads and the photon environment are weak [13–15], system-reservoir coupling terms in equation (2) and equation (3) can be safely treated perturbatively to the second order. Furthermore, under the Born–Markov approximation, the quantum master equation is given by

$$\frac{\partial}{\partial t}\hat{\rho} = -i\left[\hat{H}_D, \hat{\rho}\right] + \hat{\mathcal{L}}_e[\hat{\rho}] + \hat{\mathcal{L}}_p[\hat{\rho}], \tag{6}$$

where $\hat{\rho}$ denotes the reduced density matrix for the central DQD. The first term on the right side shows the unitary evolution of the DQD without the actions from two electronic leads and photons. The second term exhibits decoherence from the dot-lead coupling, given by (see appendix A)

$$\begin{aligned}\hat{\mathcal{L}}_e[\hat{\rho}] = \sum_{v;a=\pm} \frac{\gamma_v^a d_v^a}{2\hbar}\Big\{&\left(1 - f_v(E_a)\right)\left[|G\rangle\langle a|\hat{\rho}, \hat{d}_v^{\dagger}\right] \\ &+ f_v(E_a)\left[|a\rangle\langle G|\hat{\rho}, \hat{d}_v\right]\Big\} + \text{H.c.}\end{aligned} \tag{7}$$

$\gamma_v^a = 2\pi\sum_k \left|t_{k,v}\right|^2 \delta\left(\epsilon_{k,v} - E_a\right)$ denotes the coupling energy between the superposition state $|a\rangle$ ($|+\rangle$ or $|-\rangle$) and the lead v. In the following, we assume $\gamma_v^+ = \gamma_v^- = \gamma_v$ and set γ_v as constant in the wide band limit. The hopping matrix element $d_v^a = \langle G|\hat{d}_v|a\rangle$, originating from $\hat{d}_v(-\tau) = \sum_{\omega=E_{\pm}} e^{i\omega\tau/\hbar} d_v^a |G\rangle\langle a| + \text{H.c.}$, describes the electron transfer from the superposition state on DQD to the lead v. $f_v(E_a) = 1\Big/\left(\exp\left[\beta_v\left(E_a - \mu_v\right)\right] + 1\right)$ is the Fermi–Dirac distribution in the v lead with μ_v the corresponding chemical potential and $\beta_v = 1/\left(k_B T_v\right)$ the inverse temperature. It should be clarified that the expression of equation (7) is based on $E_- > 0$, which is equivalent to $\epsilon_L\epsilon_R > \Omega^2$. On the contrary, when $E_- < 0$ ($\epsilon_L\epsilon_R < \Omega^2$), it only needs exchange $f_v\left(E_-\right)$ with $1 - f_v\left(E_-\right)$ in equation (7). When including the external voltage bias, we conventionally set $\mu_{L(R)} = \mu_0 \pm eV_e/2$ with $\mu_0 = \left(\epsilon_L + \epsilon_R\right)/2$. This enables us to study the current-voltage characteristic of the DQDs, which is a crucial ingredient in the design of photovoltaic devices [30].

The third term depicts the effect of the photon environment on the DQD, shown as (see appendix A)

$$\hat{\mathcal{L}}_p[\hat{\rho}] = \frac{\gamma_p Q_{+-}}{2\hbar}\left\{\left(1 + n(\Lambda)\right)\left[\hat{\sigma}_-\hat{\rho}, \hat{Q}\right] + n(\Lambda)\left[\hat{\sigma}_+\hat{\rho}, \hat{Q}\right]\right\} + \text{H.c.}, \tag{8}$$

where $Q_{+-} = \langle + |\hat{Q}| - \rangle$, $\hat{\sigma}_{\pm} = |\pm\rangle\langle\mp|$ and $\hat{Q} = \hat{d}_L^{\dagger}\hat{d}_L - \hat{d}_R^{\dagger}\hat{d}_R$ describes the population polarization on the DQD. $\Lambda = E_+ - E_- = \sqrt{\Delta^2 + 4\Omega^2}$ denotes the energy gap of two eigen-levels, $\gamma_p = 2\pi\sum_k |g_k|^2\delta(\omega_k - \omega)$ is the coupling energy strength of the photon environment, and $n(\Lambda) = 1/\left[\exp(\beta_p\Lambda) - 1\right]$ is the Bose–Einstein distribution of the photon environment with β_p the inverse temperature of the sun. Clearly, only the photons with energy resonant with the eigen-level gap Λ will be absorbed. Although the current derivation of the quantum master equation is based on the eigen-state basis, it shares the same physics as in the local basis if we fully conserve the inter-dot state transitions.

Equations (7) and (8) show that eigen-states $|\pm\rangle$ of DQD are mainly responsible for the quantum transport, which is also similarly illustrated in [31]. To expose explicitly the physical picture of the photon-assisted transport, we re-express the electron–photon coupling equation (3) in the eigen-state basis as $\hat{V}_{D-ph} = \sum_q g_q\left(\hat{a}_q + \hat{a}_q^{\dagger}\right)\left(\cos\theta\hat{\tau}_z - \sin\theta\hat{\tau}_x\right)$, with $\hat{\tau}_z = |+\rangle\langle +| - |-\rangle\langle -|$ and $\hat{\tau}_x = \hat{\tau}_+ + \hat{\tau}_- = |+\rangle\langle -| + |-\rangle\langle +|$. The first term on the right side of $\hat{V}_{D-ph}$ is trivial, since it is commutative with the $\hat{H}_D$. However, for the second term, it appears as $-\sum_q \sin\theta g_q\left(\hat{a}_q^{\dagger}\hat{\tau}_- + \hat{\tau}_+\hat{a}_q\right)$ under the rotating-wave approximation. This clearly suggests that the electron hopping between $|\pm\rangle$ is assisted by the photon absorption and emission (see figure 1(b)), which makes an indispensable contribution to the appearance of the quantum photovoltaic effect in the DQD system. Moreover, it should be noted that the evolution equation of the DQD density matrix at equation (6) has no classical correspondence. This means that no electron or photon current will exhibit by studying the corresponding population dynamics under a local basis.

2.3. Electron and photon current

In the Liouville space, the density matrix of DQDs is expressed in the vector form $|\mathbb{P}\rangle = \left(\rho_{GG}, \rho_{LL}, \rho_{RR}, \rho_{LR}, \rho_{RL}\right)^T$, with $\rho_{ij} = \langle i|\hat{\rho}|j\rangle$. Then the evolution equation is re-expressed as (see appendix A):

$$\frac{\partial}{\partial t}|\mathbb{P}\rangle = \mathbb{L}|\mathbb{P}\rangle, \tag{9}$$

where $\mathbb{L}$ is the matrix form of the Liouville superoperator. The steady state solution is obtained through $\mathbb{L}|\mathbb{P}^{ss}\rangle = 0$, with $|\mathbb{P}^{ss}\rangle$ the steady state density vector. Define the direction from right to left as positive, and the photovoltaic current is obtained (see appendix B) as

$$I_e/e = \Gamma_L\rho_{LL}^{ss} - \Gamma_{GL}\rho_{GG}^{ss} + 2\Theta_{GL}\mathrm{Re}\left[\rho_{LR}^{ss}\right], \tag{10}$$

where $\Gamma_L = \frac{\gamma_L}{\hbar}\left(\cos^2\frac{\theta}{2}\left[1 - f_L(E_+)\right] + \sin^2\frac{\theta}{2}\left[1 - f_L(E_-)\right]\right)$ denotes the electron hopping rate from the left dot to the left lead; $\Gamma_{GL} = \frac{\gamma_L}{\hbar}\left(\cos^2\frac{\theta}{2}f_L(E_+) + \sin^2\frac{\theta}{2}f_L(E_-)\right)$ is the reverse-process rate from the left lead to the left dot; $\Theta_{GL} = \frac{\gamma_L\sin\theta}{4\hbar}\left(f_L(E_-) - f_L(E_+)\right)$ depicts the relaxation rate from the quantum coherent state between the left and right dots to the ground state by emitting an

electron into the left lead. This process is a pure quantum effect and gives the positive contribution to the right-to-left current. Similarly, the photon current absorbed from the solar environment can also be obtained as (see appendix B)

$$I_p = -\frac{\gamma_p \sin\theta}{2\hbar}\left(\sin\theta\left(\rho_{LL}^{ss} + \rho_{RR}^{ss}\right) + 2\left[1 + 2n(\Lambda)\right]\mathrm{Re}\left[\rho_{LR}^{ss}\right]\right). \tag{11}$$

Equations (10) and (11) imply that quantum coherence, manifested by ρ_{LR}^{ss}, is crucial to correctly describe the current. Moreover, the factor of $\sin\theta$ in I_p shows that the photon current vanishes at $\theta = 0$, i.e., at $\Omega = 0$. Accordingly, in the absence of inter-dot electron tunneling, the $|L(R)\rangle$ state keeps equilibrium with its own reservoir under the relation $\rho_{LL(RR)}^{ss}/\rho_{GG}^{ss} = \exp(-\beta_{L(R)}\Delta/2)$, which readily leads to $I_e = 0$ since the last contribution from the quantum coherence vanishes when $\Omega = 0$. On the opposite limit, when the inter-dot coupling Ω becomes large, the electron population polarization of the DQD will be small so that the electron–photon coupling becomes rather weak (see equation (3)). Moreover, increasing Ω will enhance the back-tunneling current from left to right. As a result, the photovoltaic current will be severely suppressed at large Ω. Thus, it is natural to expect maximal photovoltaic behavior in the intermediate tunneling regime.

3. Result and discussion

3.1. I–V curves

The current-voltage characteristic (*I–V* curve) is crucial for analyzing the quantum photovoltaic effect, in which the short circuit current, open circuit voltage and photovoltaic power can be explicitly identified [32–35]. We first investigate the photovoltaic current and the output power in figure 2. The temperatures of both the left and right leads are set to room temperature. For solar photons, the temperature is chosen by $T_p = 6000$ K, as traditionally described [36]. As shown in figure 2(a), when the voltage bias is turned on but small, the electron current keeps nearly the same strength as the short circuit current I_e^{sc}. However, when the voltage approaches the open circuit voltage V_{oc}, the electron current is sharply suppressed down to zero. Hence, the DQD has a high filling factor, which is crucial for high efficiency [37–39]. A similar feature has been described in other photovoltaic realizations [14, 15, 36], and is considered as a key element in the design of efficient photovoltaic devices. In recent studies regarding the cavity quantum electrodynamics system [31] and organic heterojunction [36], the photovoltaic current is exhibited as $I_e \sim 1$ pA and $I_e \sim 10$ pA, respectively. This implies that the DQD is also a promising candidate serving as the basis of the photovoltaic application.

The behavior of the photon current with the variation of voltage is similar to that of the electron current, which also exhibits large suppression near the terminal voltage. However, the terminal voltage is larger than that (V_{oc}) for the electron current (see figure 2(a)). This can be explained as follows: with finite Ω, the dot system has electron current from left to right under positive voltage in the absence of electron–photon interaction. After the electron–photon coupling is included, the photon absorption by QDs generates the electron current against the voltage bias, originating from the quantum photovoltaic effect. Therefore, the electron current is composed by two competing sources: (i) intrinsic tunneling between QDs generates downhill

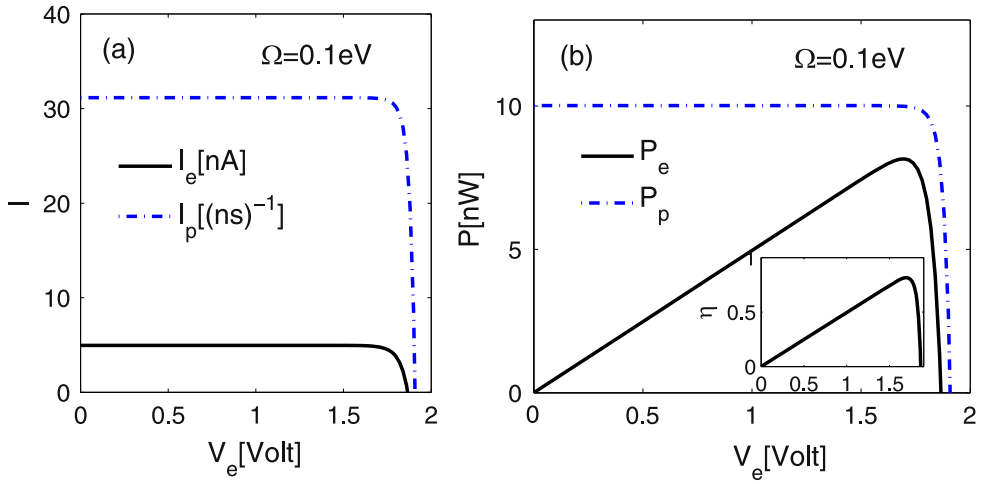

Figure 2. (a) Currents (photovoltaic current I_e and photon flow I_p) and (b) energy power (photovoltaic power P_s and solar power P_p) as functions of external voltage bias V_e. Other parameters are $\epsilon_L = 3$ eV, $\epsilon_R = 1$ eV, $\gamma_L = \gamma_R = \gamma_p = 0.1$ eV, $T_L = T_R = 300$ K and $T_p = 6000$ K.

current under positive voltage, which gives negative contribution to the electron current, and (ii) photon-generated uphill current makes a crucial positive contribution. Before the vanishing of the photon current, the photon-generated electron current will be completely eliminated by that from intrinsic inter-dot tunneling at V_{oc}, which gives the discrepancy between the two terminal voltages.

The photovoltaic (output) and solar (input) powers are studied in figure 2(b). In the small voltage bias regime, the photovoltaic power $P_e = I_e \cdot V_e$ is proportional to V_e, until reaching maximal power, since the electron current I_e remains almost constant. As the voltage reaches V_{oc}, the power suddenly drops to zero, due to the drastic diminishing of the current at V_{oc}. For the solar power $P_p = I_p \cdot \Lambda$, it is steady at the beginning, and then decays fast near the terminal voltage, which is consistent with the behavior of I_p. The maximum quantum efficiency $\eta = P_e/P_p$ of the DQD engine is then obtained near V_{oc}, as plotted on the inset in figure 2(b). This behavior is similar to photovoltaic power, and the maximal value is nearly 80%.

3.2. Effects of inter-dot quantum tunneling

Figure 3(a) shows the effect of the tunneling on the short circuit current I_e^{sc} at $V_e = 0$ in a large scale. In the weak tunneling regime, the photovoltaic current rises quickly with the increasing tunneling ($I_e^{sc} \sim \Omega^2$), which is also observed in figure 2. As the tunneling strength reaches the moderate regime, the electron current peaks at $\Omega \approx 0.55$ eV. After the peak, the current shows monotonic decay. The behavior of the photon current is similar to the electron current, except for the magnitude difference. As we discussed above, in the absence of inter-dot tunneling, two DQs are decoupled and no photon will be pumped into the dots to generate uphill current, which is clearly exhibited in equation (11). Therefore, to obtain the photovoltaic effect, finite Ω is necessary. In the opposite direction of strong tunneling, the population polarization is very small, and photons can hardly be pumped into the system due to the suppressed electron–

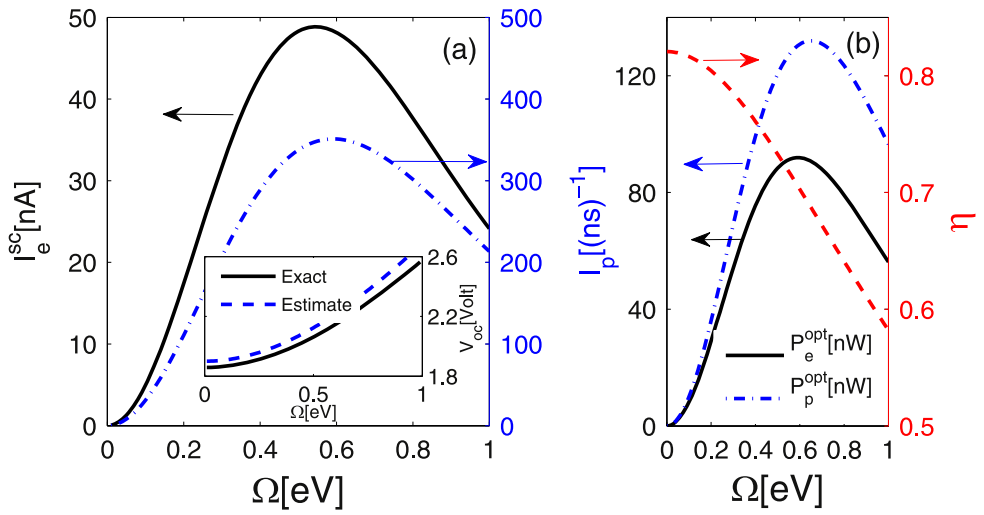

Figure 3. (a) Short circuit electron current and photon current at $V_e = 0$; the inset shows the comparison of numerically exact V_{oc} from equation (10) and the approximation estimated from equation (13). (b) Optimal output power $P_e^{\text{opt}} = \max\{I_e \cdot V\}$, corresponding input power $P_p^{\text{opt}} = I_p \cdot \Lambda$, and the efficiency $\eta = P_e^{\text{opt}}/P_p^{\text{opt}}$, as functions of electron tunneling strength Ω. Other parameters are the same as those in figure 2.

photon interaction shown in equation (3). Moreover, the strong tunneling also causes the generation of the photovoltaic current to deteriorate. Hence, it is expected that optimal tunneling will maximize the photovoltaic current, which is explicitly shown in figure 3(a).

The open circuit voltage with varying tunneling strength is also investigated in the inset of figure 3(a) (solid line), where V_{oc} shows monotonic behavior with increasing Ω that qualitatively coincides with the behavior of the eigen-level gap $\Lambda = \sqrt{\Delta^2 + 4\Omega^2}$. This can be understood as follows: When the inter-dot tunneling Ω is weak, it is known that $\sin\theta \approx 0 (\cos\theta \approx 1)$ so that $|+\rangle$ only effectively connects to the left lead and $|-\rangle$ effectively couples with the right lead (see A.6, A.7, A.8, A.9)). Besides, the eigen-levels $|+\rangle$ and $|-\rangle$ are nearly uncoupled since they become orthogonal to each other. The tunneling between them is mainly assisted by the photon-induced excitation and relaxation. Hence at the open circuit voltage, considering electron pump from the right ($|-\rangle$) to the left ($|+\rangle$) is balanced by the reverse action, we have the detailed balance relation:

$$\frac{f_L(E_+)}{1 - f_L(E_+)} \times \frac{1 + n_p(\Lambda)}{n_p(\Lambda)} \times \frac{1 - f_R(E_-)}{f_R(E_-)} = 1, \tag{12}$$

where the rate from the left lead to the right one is proportional to $f_L(E_+)\left[1 + n_p(\Lambda)\right]\left[1 - f_R(E_-)\right]$, while the reverse rate from right to left is proportional to $\left[1 - f_L(E_+)\right] n_p(\Lambda) f_R(E_-)$. This detailed balance relation finally gives us

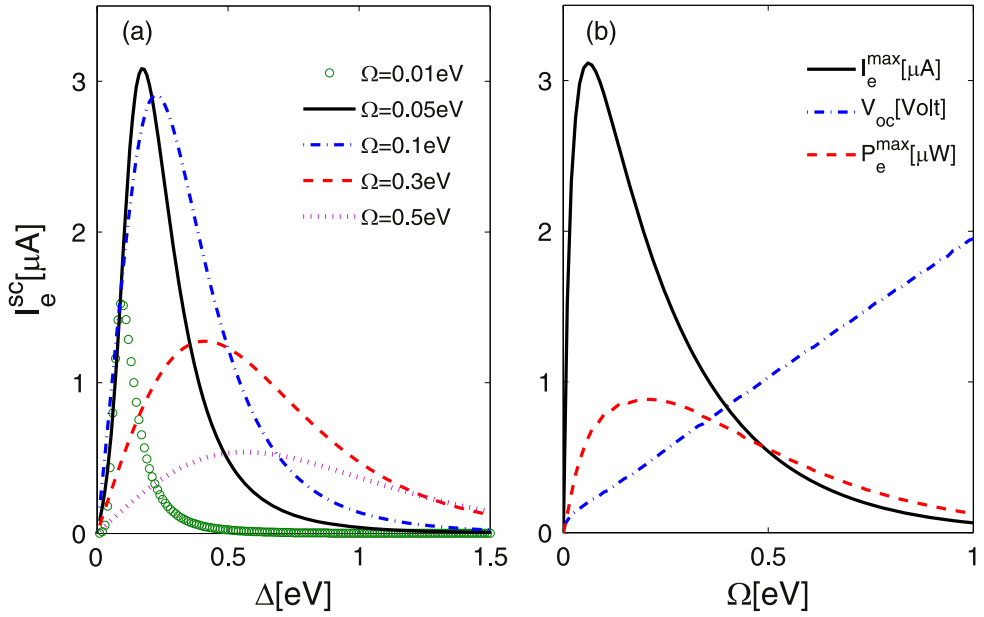

Figure 4. (a) Short circuit current as a function of Δ with different Ω. (b) Maximum of the photovoltaic current, the corresponding open circuit voltage and output power, under various Ω. Other parameters are the same as those in figure 2.

$$V_{oc} = \frac{\Lambda}{e}\left(1 - \frac{T_0}{T_p}\right), \tag{13}$$

where $T_{0(p)}$ denotes the electronic reservoirs (solar environment) temperature and $1 - T_0/T_p$ is the ideal Carnot efficiency. This rough estimation qualitatively agrees with the numerical exact result in the inset of figure 3(a), and the slight deviation comes from the weak inter-dot tunneling, which reduces V_{oc} compared to the ideal one at equation (13). From these results, it is interesting to find that below the optimal tunneling ($\Omega \approx 0.55$ eV in our case), both the photovoltaic current and voltage are enhanced by the tunneling strength. Thus, the best operation regime is around the optimal tunneling, where the maximum output power will be obtained. This feature is explicitly shown in figure 3(b). However, the photovoltaic efficiency corresponding to the maximal extractable output power is not the largest, which shows monotonic decay. This provides useful guidance to optimize the quantum photovoltaic effect.

3.3. Global optimal performance

Next, we study the effect of the inter-dot energy gap Δ on the photovoltaic current in figure 4(a). For arbitrary tunneling strength, there always exists an optimal gap to maximize the current. Moreover, the overall profiles are similar: the current firstly arises with increasing Δ, and then it decays monotonically after reaching the maximum. However, the differences are also apparent. For weak tunneling, i.e., $\Omega = 0.01$ eV, the value of the peak is small at around 1.5 μA. As the tunneling is strengthened, this value becomes large, i.e., $I_e^{\max} \approx 3\ \mu$A. When the tunneling is further increased, the current again becomes weak. Besides, the peak is broadened with increasing Ω. Based on the results of figure 4(a), we extract the maximum values of the current

($I_e^{\max}$) and investigate their dependence on the tunneling strength, shown in figure 4(b). The global summit appears at $\Omega \approx 0.08$ eV, which corresponds to the gap of two excited states $\Lambda \approx 0.3$ eV. Hence the central frequency of the absorption photons is in the infrared regime [11], and the maximum value of the current can be as large as 3 μ A. It shows competitive improvement by comparison with photovoltaic current in other photocell units, i.e., $I_{sc} \sim 1$ pA in [31] and $I_{sc} \sim 10$ pA in [36].

In the case of open circuit voltage corresponding to maximum short circuit current, it changes almost linearly with Ω (we also find an excellent linear relation of V_{oc} with Λ) [40, 41], which is quite different from that in figure 3(b). The difference mainly comes from the different flexibility of the energy bias Δ. For the formal case in figure 3(b), the energy bias is fixed with $\Delta = 2$ eV, and does not change with the variation of Ω. However, for the present case, the maximum electron current shows the global picture in the parameter space of Δ and Ω, where Δ is adjusted with varying Ω. We also investigate the maximum power, defined as $P_e^{\max} = I_e^{\max} \cdot V_{oc}$. This also shows the peak effect with optimal tunneling, but the optimal point deviates from that for the photovoltaic current. As is well-known, over 50% of solar energy is below the visible light spectrum [42]. Therefore, our results suggest that it is meaningful to use the DQD as one basis for the design of efficient solar energy harvesters.

4. Conclusion

In summary, we have studied the quantum photovoltaic effect in a DQD system weakly coupled to electronic leads and a solar environment by applying the quantum master equation. Three main ingredients of photovoltaic effect—short circuit current, open circuit voltage and output power—have been analyzed in detail. As the voltage bias approaches open circuit voltage (V_{oc}), the electron current is strongly suppressed to zero, implying the high fill factor. In comparison, the photon current is eliminated at a larger terminal voltage. This discrepancy mainly originates from the fact that the photovoltaic current is composed by two competing sources: one from the photon-generated uphill electron current against the potential bias, and the other from the voltage bias driving the electron current along the potential gradient. When the photovoltaic current disappears, these currents induced from two sources are equal, resulting in the finite photon current. Moreover, the photovoltaic current and power are much larger than other recently studied nano-junction photovoltaic systems, which is crucial for designing photovoltaic devices.

The influence of the inter-dot tunneling strength on the photovoltaic current is investigated. The optimal tunneling to maximize the photovoltaic current has been found in the intermediate regime, whose character should be intrinsic in this kind of system. However, the open circuit voltage increases monotonically with increasing tunneling, which can be qualitatively described by $V_{oc} \sim \Lambda\left(1 - T_0/T_p\right)$, based on the detailed balance condition. The global optimal tunneling to achieve maximal photovoltaic current and power has also been exhibited, with the central frequency of absorption photons in the infrared regime. We believe that these results provide a theoretical basis for promising photovoltaic applications of DQDs.

Acknowledgments

This work was supported by the National Science Foundation (NSF) (grant no. CHE-1112825) and the Defense Advanced Research Projects Agency (DARPA) (grant no. N99001-10-1-4063). CW has been supported by the Singapore-MIT Alliance for Research and Technology (SMART). JR acknowledges the auspices of the National Nuclear Security Administration of the US DOE at LANL under contract no. DE-AC52-06NA25396, through the LDRD Program. JC has been supported by the Center for Excitonics, an Energy Frontier Research Center funded by the US Department of Energy, Office of Science, Office of Basic Energy Science.

Appendix A. The quantum master equation under the counting field

To derive the electron current and the photon flow, we usually include the counting field as in the method of full counting statistics [43–46]. Here, we count the electron number $\hat{N}_L = \sum_k \hat{c}^\dagger_{k,L}\hat{c}_{k,L}$ on the left fermion reservoir and the photon number $\hat{N}_p = \sum_k \hat{a}^\dagger_k \hat{a}_k$ in the solar environment. The Hamiltonian of the whole system is modified to [28]

$$\begin{aligned}\hat{H}_\chi &= e^{i\left(\hat{N}_L\chi_e+\hat{N}_p\chi_p\right)/2}\hat{H}e^{-i\left(\hat{N}_L\chi_e+\hat{N}_p\chi_p\right)/2}\\ &= \hat{H}_D + \sum_{v=L,R}\left(\hat{V}_v^{\chi_e}+\hat{H}_v\right) + \hat{V}_{D-ph}^{\chi_p} + \hat{H}_{ph},\end{aligned} \tag{A.1}$$

where $\chi = \left(\chi_e, \chi_p\right)$ count the currents transferring into the corresponding reservoirs, and the system-bath interactions are modified to

$$\begin{aligned}\hat{V}_v^{\chi_e} &= \sum_{k,v} t_{k,v} e^{-i\chi_e\delta_{v,L}/2}\hat{d}_v^\dagger \hat{c}_{k,v} + \text{H.c.},\\ \hat{V}_{D-ph}^{\chi_p} &= \sum_q g_q\left(\hat{a}_q e^{-i\chi_p/2} + \hat{a}_q^\dagger e^{i\chi_p/2}\right)\left(\hat{d}_L^\dagger\hat{d}_L - \hat{d}_R^\dagger\hat{d}_R\right),\end{aligned}$$

with $\delta_{\alpha,\beta} = 1$ if $\alpha = \beta$, otherwise $\delta_{\alpha,\beta} = 0$. Following the standard procedure treated in the quantum master equation, including the counting the field up to the second order [28, 46, 47], the dissipator from the QD-electron reservoir is derived as

$$\begin{aligned}\hat{\mathcal{L}}_e\left[\hat{\rho}_\chi\right] = \sum_{v,a}\frac{\gamma_v^a d_{v,Ga}}{2\hbar}\Big\{&f_v\left(E_a\right)e^{-i\chi_e\delta_{v,L}}\left(\hat{d}_v^\dagger\hat{\rho}|G\rangle\langle a| + \text{H.c.}\right)\\ &+\left(1-f_v\left(E_a\right)\right)e^{i\chi_e\delta_{v,L}}\left(\hat{d}_v\hat{\rho}|a\rangle\langle G| + \text{H.c.}\right)\\ &-\left(\left[\left(1-f_v\left(E_a\right)\right)\hat{d}_v^\dagger|G\rangle\langle a|\hat{\rho} + f_v\left(E_a\right)\hat{d}_v|a\rangle\langle G|\hat{\rho}\right] + \text{H.c.}\right)\Big\},\end{aligned} \tag{A.2}$$

with $v = L, R$ and $a = \pm$. It will naturally reduce to equation (7) when $\chi_e = 0$. The Liouville operator from the dot-photon coupling is shown as

$$\hat{\mathcal{L}}_p\left[\hat{\rho}_\chi\right] = \frac{\gamma_p Q_{+-}}{2\hbar}\Big\{ n(\Lambda)e^{-i\chi_p}\left(\hat{Q}\hat{\rho}|-\rangle\langle+| + \text{H.c.}\right) + \left(1+n(\Lambda)\right)e^{i\chi_p}\left(\hat{Q}\hat{\rho}|+\rangle\langle-| + \text{H.c.}\right) - \left(\left[\left(1+n(\Lambda)\right)\hat{Q}|-\rangle\langle+|\hat{\rho} + n(\Lambda)\hat{Q}|+\rangle\langle-|\hat{\rho}\right] + \text{H.c.}\right)\Big\}. \tag{A.3}$$

When $\chi_p = 0$, it returns back to equation (8) consistently. Then the quantum master equation under the counting field is described by

$$\frac{\partial}{\partial t}\hat{\rho}_\chi = -i\left[\hat{H}_D, \hat{\rho}_\chi\right] + \hat{\mathcal{L}}_e\left[\hat{\rho}_\chi\right] + \hat{\mathcal{L}}_p\left[\hat{\rho}_\chi\right]. \tag{A.4}$$

Furthermore, in the Liouville space the reduced density matrix of the DQD system is expressed as vector form $|\mathbb{P}_\chi\rangle = \left(\rho_{GG}, \rho_{LL}, \rho_{RR}, \rho_{LR}, \rho_{RL}\right)^T$, with $\rho_{ij} = \langle i|\hat{\rho}_\chi|j\rangle$. Hence, the corresponding evolution equation of the DQD density matrix is given by

$$\frac{\partial}{\partial t}|\mathbb{P}_\chi\rangle = \mathbb{L}_\chi|\mathbb{P}_\chi\rangle, \tag{A.5}$$

with $\mathbb{L}_\chi = \mathbb{L}^e_{\chi_e} + \mathbb{L}^p_{\chi_p}$. When $\chi_e = \chi_p = 0$, equation (A.5) is just simplified back to equation (9) with $\left|\mathbb{P}_\chi\right\rangle$ reducing to $|\mathbb{P}\rangle$ and $\mathbb{L}_\chi$ reducing to $\mathbb{L}$. Here $\mathbb{L}^e_{\chi_e}$ describes the superoperator for the electron leads induced decoherence as

$$\mathbb{L}^e_{\chi_e} = \begin{pmatrix} -(\Gamma_{GL}+\Gamma_{GR}) & \Gamma_L e^{i\chi_e} & \Gamma_R & \Theta_{GL}e^{i\chi_e}+\Theta_{GR} & \Theta_{GL}e^{i\chi_e}+\Theta_{GR} \\ \Gamma_{GL}e^{-i\chi_e} & -\Gamma_L & 0 & -\Theta_{GL}+i\Omega & -\Theta_{GL}-i\Omega \\ \Gamma_{GR} & 0 & -\Gamma_R & -\Theta_{GR}-i\Omega & -\Theta_{GR}+i\Omega \\ \Gamma^e_{\chi_e} & -\Theta_{GR}+i\Omega & -\Theta_{GL}-i\Omega & -\frac{\Gamma_L+\Gamma_R}{2}-i\Delta & 0 \\ \Gamma^e_{\chi_e} & -\Theta_{GR}-i\Omega & -\Theta_{GL}+i\Omega & 0 & \frac{\Gamma_L+\Gamma_R}{2}+i\Delta \end{pmatrix},$$

where $\Delta = \epsilon_L - \epsilon_R$, and the other renormalized parameters are explicitly given by

$$\Gamma_{GL} = \frac{\gamma_L}{\hbar}\left(\cos^2\frac{\theta}{2}f_L(E_+) + \sin^2\frac{\theta}{2}f_L(E_-)\right), \tag{A.6}$$

$$\Gamma_{GR} = \frac{\gamma_R}{\hbar}\left(\sin^2\frac{\theta}{2}f_R(E_+) + \cos^2\frac{\theta}{2}f_R(E_-)\right), \tag{A.7}$$

$$\Gamma_L = \frac{\gamma_L}{\hbar}\left(\cos^2\frac{\theta}{2}\left[1-f_L(E_+)\right] + \sin^2\frac{\theta}{2}\left[1-f_L(E_-)\right]\right), \tag{A.8}$$

$$\Gamma_R = \frac{\gamma_R}{\hbar}\left(\sin^2\frac{\theta}{2}\left[1-f_R(E_+)\right] + \cos^2\frac{\theta}{2}\left[1-f_R(E_-)\right]\right), \tag{A.9}$$

$$\Theta_{GL(GR)} = \frac{\sin\theta\gamma_{L(R)}}{4\hbar}\Big(f_{L(R)}(E_-) - f_{L(R)}(E_+)\Big), \tag{A.10}$$

$$\Gamma^e_{\chi_e} = \frac{\sin\theta}{4\hbar}\Big(\gamma_L\Big[f_L(E_+) - f_L(E_-)\Big]e^{-i\chi_e} + \gamma_R\Big[f_R(E_+) - f_R(E_-)\Big]\Big). \tag{A.11}$$

While $\mathbb{L}^{\,p}_{\chi_p}$ accounts for the electron–photon interaction, shown as

$$\mathbb{L}^{\,p}_{\chi_p} = \begin{pmatrix} 0 & 0 & 0 & 0 & 0 \\ 0 & -\Gamma^p_{\chi_p} & 0 & -\Gamma^p_{L,\chi_p} & -\Gamma^p_{L,\chi_p} \\ 0 & 0 & -\Gamma^p_{\chi_p} & -\Gamma^p_{R,\chi_p} & -\Gamma^p_{R,\chi_p} \\ 0 & -\Theta^1_{\chi_p} & -\Theta^2_{\chi_p} & -\Theta^3_{\chi_p} & 0 \\ 0 & -\Theta^1_{\chi_p} & -\Theta^2_{\chi_p} & 0 & -\Theta^3_{\chi_p} \end{pmatrix}, \tag{A.12}$$

with the elements

$$\Gamma^p_{\chi_p} = \frac{\gamma_p \sin^2\theta}{2\hbar}\Big(\Big[1 + 2n(\Lambda)\Big] - n(\Lambda)e^{-i\chi_p} - \Big[1 + n(\Lambda)\Big]e^{i\chi_p}\Big), \tag{A.13}$$

$$\Gamma^p_{L,\chi_p} = \frac{\sin\theta\gamma_p}{2\hbar}\Big[\sin^2\frac{\theta}{2}\Big[1 + n(\Lambda)\Big]\Big(1 - e^{i\chi_p}\Big) - \cos^2\frac{\theta}{2}n(\Lambda)\Big(1 - e^{-i\chi_p}\Big)\Big], \tag{A.14}$$

$$\Gamma^p_{R,\chi_p} = \frac{\sin\theta\gamma_p}{2\hbar}\Big(\cos^2\frac{\theta}{2}\Big[1 + n(\Lambda)\Big]\Big(1 - e^{i\chi_p}\Big) - \sin^2\frac{\theta}{2}n(\Lambda)\Big(1 - e^{-i\chi_p}\Big)\Big), \tag{A.15}$$

$$\Theta^1_{\chi_p} = \frac{\sin\theta\gamma_p}{2\hbar}\Big(\cos^2\frac{\theta}{2}\Big[1 + n(\Lambda)\Big]\Big(1 + e^{i\chi_p}\Big) - \sin^2\frac{\theta}{2}n(\Lambda)\Big(1 + e^{-i\chi_p}\Big)\Big), \tag{A.16}$$

$$\Theta^2_{\chi_p} = \frac{\sin\theta\gamma_p}{2\hbar}\Big(\sin^2\frac{\theta}{2}\Big[1 + n(\Lambda)\Big]\Big(1 + e^{i\chi_p}\Big) - \cos^2\frac{\theta}{2}n(\Lambda)\Big(1 + e^{-i\chi_p}\Big)\Big), \tag{A.17}$$

$$\Theta^3_{\chi_p} = \frac{\sin^2\theta\gamma_p}{2\hbar}\Big(\Big[1 + 2n(\Lambda)\Big] + n(\Lambda)e^{-i\chi_p} + \Big[1 + n(\Lambda)\Big]e^{i\chi_p}\Big). \tag{A.18}$$

Appendix B. Derivation of the currents

From the evolution equation $\frac{\partial}{\partial t}|\mathbb{P}_\chi\rangle = \mathbb{L}_\chi|\mathbb{P}_\chi\rangle$, we can define the characteristic function

$$\mathcal{Z}(\chi, t) = \langle 1|\mathbb{P}_\chi(t)\rangle = \langle 1|e^{\mathbb{L}_\chi t}|\mathbb{P}_\chi(0)\rangle, \tag{B.1}$$

where $\langle 1| = \big(1, 1, 1, 0, 0\big)$ considering $\rho_{GG} + \rho_{LL} + \rho_{RR} = 1$. In the long time limit, the cumulant generating function can then be expressed as [48, 49]

$$\mathcal{G}(\chi) = \lim_{t\to\infty}\frac{1}{t}\mathcal{Z}(\chi, t) = \lambda_0(\chi), \tag{B.2}$$

where $\lambda_0(\chi)$ is the eigen-value of the operator $\mathbb{L}_\chi$, which has the largest real part and thus dominates the dynamics in the steady state. The current is just the first order cumulant that is then obtained by the first order derivative

$$\mathcal{I} := \left.\frac{\partial \mathcal{G}(\chi)}{\partial(i\chi)}\right|_{\chi=0} = \left.\frac{\partial \lambda_0(\chi)}{\partial(i\chi)}\right|_{\chi=0} = \left\langle 1 \left| \left.\frac{\partial \mathbb{L}_\chi}{\partial(i\chi)}\right|_{\chi=0} \right| \mathbb{P}^{ss} \right\rangle. \tag{B.3}$$

For the specific current calculation, $\chi = \chi_e$ gives the electron current, and $\chi = \chi_p$ gives the photon flow.

Therefore, the electron current is obtained as

$$\begin{aligned} I_e/e &= \left\langle 1 \left| \left.\frac{\partial \mathbb{L}^{e}_{\chi_e}}{\partial(i\chi_e)}\right|_{\chi_e=0} \right| \mathbb{P}^{ss} \right\rangle \\ &= \Gamma_L \rho^{ss}_{LL} - \Gamma_{GL} \rho^{ss}_{GG} + 2\Theta_{GL} \mathrm{Re}\left[\rho^{ss}_{LR}\right], \end{aligned} \tag{B.4}$$

where $|\mathbb{P}^{ss}\rangle$ is the vector of the density matrix in a steady state. Similarly, the photon flow out of the environment can also be obtained as

$$\begin{aligned} I_p &= -\left\langle 1 \left| \left.\frac{\partial \mathbb{L}^{p}_{\chi_p}}{\partial(i\chi_p)}\right|_{\chi_p=0} \right| \mathbb{P}^{ss} \right\rangle \\ &= -\frac{\gamma_p}{2}\left(\sin^2\theta\left(\rho^{ss}_{LL} + \rho^{ss}_{RR}\right) + 2\sin\theta\left(1 + 2n(\Lambda)\right)\mathrm{Re}\left[\rho^{ss}_{LR}\right]\right). \end{aligned} \tag{B.5}$$

Since the counting field counts the photon current into the reservoir, there is a minus sign for calculating the photon current out of the reservoir.

References

[1] Tiwari G N 2002 *Solar Energy: Fundamentals, Design, Modelling and Applications* (New Delhi: Narosa)

[2] Green M A, Emery K, Hishikawa Y, Warta W and Dunlop E D 2009 *Prog. Photovoltaics* **17** 320
Green M A, Emery K, Hishikawa Y and Warta W 2009 *Prog. Photovoltaics* **18** 144
Green M A, Emery K, Hishikawa Y and Warta W 2009 *Prog. Photovoltaics* **20** 606

[3] Wolf M 1960 *Proc. IRE* **48** p 1246

[4] Shockley W and Queisser H J 1961 *J. Appl. Phys.* **32** 510

[5] Ross R T and Nozik A J 1982 *J. Appl. Phys.* **53** 3813
Nozik A J 2002 *Physica* E **14** 115

[6] Sano N and Yoshii A 1992 *Phys. Rev.* B **45** 4171

[7] Kolodinski S, Werner J H, Wittchen T and Queisser H J 1993 *Appl. Phys. Lett.* **63** 2405

[8] Werner J H, Kolodinski S and Queisser H J 1994 *Phys. Rev. Lett.* **74** 3851

[9] Brendel R, Werner J H and Queisser H J 1996 *Sol. Energy Mater. Sol. Cell* **41** 419

[10] Chanyawadee S, Harley R T, Henini M, Talapin D V and Lagoudakis P G 2009 *Phys. Rev. Lett.* **102** 077402

[11] Sablon K A, Little J W, Mitin V, Sergeev A, Vagidov N and Reinhardt K 2011 *Nano Lett.* **11** 2311

[12] Nozik A J 2010 *Nano. Lett.* **10** 2735
[13] Scully M O 2010 *Phys. Rev. Lett.* **104** 207701
[14] Scully M O, Chapin K R, Dorfman K E, Kim M B and Svidzinsky A 2011 *Proc. Natl Acad. Sci. USA* **108** 15097
[15] Dorfman K E, Voronine D V, Mukamel S and Scully M O 2013 *Proc. Natl Acad. Sci. USA* **110** 2746
[16] Nalbach P and Thorwart M 2013 *Proc. Natl Acad. Sci. USA* **110** 2693
[17] Cao J and Silbey R J 2009 *J. Phys. Chem.* A **113** 13825
[18] Wu J, Liu F, Shen Y, Cao J and Silbey R J 2010 *New J. Phys.* **12** 105012
[19] Wu J, Liu F, Ma J, Silbey R J and Cao J 2012 *J. Chem. Phys.* **137** 174111
[20] Wu J, Silbey R J and Cao J 2013 *Phys. Rev. Lett.* **110** 200402
[21] van der Wiel W G, de Franceschi S, Elzerman J M, Fujisawa T, Tarucha S and Kouwenhoven L P 2002 *Rev. Mod. Phys.* **75** 1
[22] Delbecq M R, Schmitt V, Parmentier F D, Roch N, Viennot J J, Fève G, Huard B, Mora C, Cottet A and Kontos T 2011 *Phys. Rev. Lett.* **107** 256804
[23] Delbecq M R, Bruhat L E, Viennot J J, Datta S, Cottet A and Kontos T 2013 *Nat. Commun.* **4** 1400
[24] Fujisawa T, Oosterkamp T H, van der Wiel W G, Broer B W, Aguado R, Tarucha S and Kouwenhoven L P 1998 *Science* **282** 932
[25] Brandes T and Vorrath T 2002 *Phys. Rev.* B **66** 075341
[26] Kießlich G, Schöll E, Brandes T, Hohls F and Haug R J 2007 *Phys. Rev. Lett.* **99** 206602
[27] Rozbicki E and Machnikowski P 2008 *Phys. Rev. Lett.* **100** 027401
[28] Wang C, Ren J, Li B and Chen Q H 2012 *Eur. Phys. J.* B **85** 110
[29] Kosloff R 2013 *Entropy* **15** 2100
[30] Masters G M 2004 *Renewable and Efficient Electric Power System* (Hoboken, NJ: Wiley)
[31] Xu C R and Vavilov M G 2013 *Phys. Rev.* B **87** 035429
[32] Chen H Y, Hou J H, Zhang S Q, Liang Y Y, Yang G W, Yang Y, Yu L P and Li G 2009 *Nat. Photon.* **3** 649
[33] Shalom M, Dor S, Rühle S, Grinis L and Zaban A 2009 *J. Phys. Chem.* C **113** 3895
[34] Kamat P V, Tvrdy K, Baker D R and Radich J G 2010 *Chem. Rev.* **110** 6664
[35] Tang J and Sargent E H 2012 *Adv. Mater.* **23** 12
[36] Einax M, Dierl M and Nitzan A 2011 *J. Phys. Chem.* C **115** 21396
[37] Dou L T, You J B, Yang J, Chen C C, He Y J, Murase S, Moriarty T, Emery K, Li G and Yang Y 2012 *Nat. Photon.* **6** 180
Li G, Zhu R and Yang Y 2012 *Nat. Photon.* **6** 153
[38] He Z C, Zhong C M, Su S J, Xu M, Wu H B and Cao Y 2012 *Nat. Photon.* **6** 591
[39] He Z C, Zhang C M, Huang X, Wong W Y, Wu H B, Chen L W, Su S J and Cao Y 2011 *Adv. Mater.* **23** 4636
[40] Yoon W J, Boercker J E, Lumb M P, Placencia D, Foos E E and Thschler J G 2013 *Sci. Rep.* **3** 2225
[41] Scharber M C, Mühlbacher D, Koppe M, Denk P, Waldauf C, Heeger A J and Brabec C J 2006 *Adv. Mater.* **18** 789
[42] Moore G F and Brudvig G W 2011 *Annu. Rev. Condens. Matter Phys.* **2** 303
[43] Büttiker Y M and lanter M 2000 *Phys. Rep.* **336** 1
[44] Levitov L S and Vesovik G 1993 *JETP Lett.* **58** 230
[45] Levitov L S, Lee H and Lesovik G B 1996 *J. Math. Phys.* **37** 4845
[46] Esposito M, Harbola U and Mukamel S 2009 *Rev. Mod. Phys.* **81** 1665
[47] Yuge T, Sagawa T, Sugita A and Hayakawa H 2012 *Phys. Rev.* B **86** 235308
[48] Ren J, Hänggi P and Li B 2010 *Phys. Rev. Lett.* **104** 170601
[49] Ren J, Liu S and Li B 2012 *Phys. Rev. Lett.* **108** 210603